Environmental Research 186 (2020) 109484

Contents lists available at ScienceDirect

Environmental Research

journal homepage: www.elsevier.com/locate/envres

Removal of Basic Fuchsin from water by using mussel powdered eggshell membrane as novel bioadsorbent: Equilibrium, kinetics, and thermodynamic studies

Wahiba Bessashia[a,b], Yamina Berredjem[a], Zhour Hattab[b], Mohamed Bououdina[c,*]

[a] Science and Technology Laboratory of Water and Environment, Department of Material Sciences, Faculty of Sciences and Technology, Mohammed Cherif Messaadia University, Souk Ahras, 41000, Algeria

[b] Laboratory of Water Treatment and Valorization of Industrial Wastes, Department of Chemistry, Faculty of Sciences, University Badji Mokhtar, B.P. 12, Annaba, 23000, Algeria

[c] Department of Physics, College of Science, University of Bahrain, PO Box 32038, Bahrain

ARTICLE INFO

Keywords:
Adsorption
Basic Fuchsin
Eggshell membrane
Kinetics
Thermodynamic

ABSTRACT

This study aims to remove organic cationic dye Basic Fuchsin (BF) by adsorption onto a low cost eggshell membrane (ESM) in batch mode at 293 K. XRD analysis confirms the amorphous nature of ESM meanwhile FTIR spectroscopy reveals the presence of several functional groups such as hydroxyl (–OH), sulfhydryl (–SH), carboxyl (–COOH), and amino ($–NH_2$). Morphological observations by SEM indicate its fibrous microstructure. BET analysis shows a surface area of 11.56 $m^2\ g^{-1}$ and the presence of mesopores with a volume of 6.173 10^{-3} $cm^3\ g^{-1}$. The value of pH_{PZC} of ESM is 7.05. The influence of adsorbent dose, contact time, pH, temperature and dye concentration is examined. The highest adsorption capacity around 48 $mg.g^{-1}$is achieved for a dye concentration 250 ppm, pH 6 and 25 °C. In addition, adsorption has been found to follow pseudo-second order kinetics. The analysis of the experimental data using linear forms based on Langmuir, Freundlich and Temkin isotherm models indicate that the best fit is obtained with Freundlich model. Thermodynamic parameters (Gibbs free energy, enthalpy, and entropy) reveal that the adsorption of BF onto ESM is an exothermic and spontaneous process. A comprehensive mechanism for BF adsorption by ESM has been proposed.

1. Introduction

Dyes from various species of the chemical industry were considered the main component of wastewater (Bayramoglu et al., 2009). Nowadays, a large variety of dyes is widely used and discarded, in most cases, without preliminary treatment, thereby causing pollution and environmental concerns. It has been reported that the textile industry consumes more than 700,000 tons of dyes accounting of around 10,000 types; one of major's pollutants (Li et al., 2018a).Compared to anionic dyes, the cationic dyes have been identified more toxic, with relatively high tinctorial values (less than 1.0 mg/L) (Bayramoglu et al., 2009).

Basic Fuchsin, defined as a complex red phenyl methane dye, contains mainly three components namely pararosaniline, rosaniline, and magenta II (Kong et al., 2014; Zeyada et al., 2015). It is utilized in numerous applications, including but not limited to, tissue-specific staining of biological and coloring materials like cotton, orlon, paper and leather (Qin et al., 2014), biological stain for nucleus, tissues and muscles in addition as tracking certain proteins (Kalita et al., 2017). Considering its toxicity and carcinogenic effects alongside with a poor biodegradation, the removal of BF from wastewater becomes necessary in order to reduce or eliminate it before being discharged in natural medium (El Haddad, 2016). Herein, it is important to highlight that environment protection requires profound awareness regarding the use of dyes alongside with law enforcement through governmental and non-governmental agencies.

Numerous wastewater decolorization techniques can be applied such as coagulation– flocculation (Verma et al., 2012), chemical treatment (Uliana et al., 2012), aerobic and anaerobic biological treatments (El-Khateeb et al., 2009), advanced oxidation processes like Fenton and photocatalysis (Quadrado and Fajardo 2017; Wang et al., 2014; Saleh and Taufik 2019) as well as adsorption (Postai et al., 2016; Asfaram et al., 2017).Each technique offers specific application with distinct advantages and drawbacks. Generally speaking, the adopted method is usually evaluated according several factors, including its cost, application and performance relative to the desired aim. The adsorption is considered as one of the most advantageous process for

* Corresponding author.
E-mail address: mboudina@gmail.com (M. Bououdina).

https://doi.org/10.1016/j.envres.2020.109484
Received 10 February 2020; Received in revised form 30 March 2020; Accepted 1 April 2020
Available online 08 April 2020
0013-9351/

water and wastewater decolorization due to its efficiency, low cost and simplicity (Rahman and Khan, 2016). Meanwhile, the granular activated carbon is recognized as abundant and thereby the most used adsorbent for water treatment. However, it has been reported to present some limitations such as its costly chemical and thermal regeneration.

On the hand side, biomaterials are now widely studied as future promising adsorbent, mainly because of their abundance, environmental friendly and the possibility to be produced from renewable sources. Recently, many researchers have been interested in the preparation of biosorbents and investigate their properties in addition to their efficiency for the removal of several organic contaminants, such as sugarcane bagasse (Sadaf et al., 2014), phoenix tree leaf (Han et al., 2009), food residues as coffee grounds (Kyzas et al. 2012; Shen and Gondal 2017) eggshell membrane (Abdel-Khalek et al., 2017; Liu and Liu, 2011; Pramanpol and Nitayapat, 2006) and lignocellulosic materials (Khelaifia et al., 2016; Nouacer et al., 2016). Consequently, the adopted methodology becomes cost-effective meanwhile contributes to sustainable development through the valorization of natural materials and industrial wastes.

In this study, eggshell membrane (ESM) as potential bioadsorbent has been investigated for the removal of basic Fuchsin (BF) dye from aqueous solutions. The eggshell membrane, representing the thin layer between the egg white and the shell, is composed of porous network of insoluble fibrous proteins with a relatively large surface area and could be considered as a promising sorbent for organic contaminants from wastewater (Wang et al., 2010; Torres et al., 2010).

Generally speaking, eggshell, as natural biomaterial, has been used for diverse applications such as catalysts for volatile organic compounds (VOCs) oxidation (Li et al., 2020), semiconductors (Zhang et al., 2020b), low-cost photocatalysts (Zhang et al., 2020a), photocatalysis and antibacterial (Zhang et al., 2019), as well detector and catalyst (Ding et al., 2020).

Particularly, eggshell membrane has been found to offer promising applications including: bioinspired carbon dots (Choi and Zheng, 2019),on-enzymatic electrochemical dopamine sensor (Liu et al., 2020), high-performance electrode materials (Chung and Manthiram, 2014), biosensor (D'Souza et al., 2013), antibacterial (Liu et al., 2017; He et al., 2019; Li et al., 2019), detector (Cao et al., 2020), catalysis (Li et al., 2017a), photocatalysis (Preda et al., 2020), supercapacitor (da Silva et al., 2019), medicinal products and biomaterial for wound care dressing (Li et al., 2018b), as well adsorbent (He et al., 2019).

Some research groups (Ummartyotin et al., 2016; Abdel-Khalek et al., 2017) have investigated the efficiency of ESM as an adsorbent for the removal of dyes and heavy metals from water. On the other hand, because of its biocompatible nature, the ESM can be easily degraded after its use, resulting in less secondary waste. The main objective of this research work consists on determining the adsorption performance of BF in batch mode.

Based on the literature review and to the best knowledge of authors, no previous studies in the literature have been conducted to establish the adsorption of BF in wastewater by using ESM as bioadsorbent. Nevertheless, it is important to mention that ESM has been studied in the field of water treatment (Gupta et al., 2008; El Haddad, 2016). The eggshell membrane is defined as a dual membrane with an intricate lattice meshwork of interlocked large and small fibers forming a tenacious sheath. The two membranes are simply separated by mechanical dissection, due to plane cleavage existing between these two layers.

ESM fibers are composed mainly of proteins (80–85%) and a small amount of polysaccharide; the protein which approximately 10% are collagens (types I, V and X) and 70–75% of other proteins and glycoproteins (Baláž, 2014; Tsai et al., 2006).

This study aims to determine the corresponding effects associated with the variation of experimental parameters, namely the adsorbent dose, contact time, stirring speed, temperature, pH and dye initial concentration. Additionally, numerical analysis is carried out in order to elucidate the adsorption kinetics by two main models; i.e. pseudo first-order and pseudo-second-order. Meanwhile, the equilibrium data will be modeled using three equations: Langmuir, Freundlich and Temkin. The thermodynamic parameters for the adsorption of BF ions are also determined.

2. Materials and methods

2.1. Chemicals

The basic fuchsin (BF) was dissolved in double distilled water (DDW) to prepare a stock solution of 1000 $mg.L^{-1}$, and then a series of diluted solutions were prepared with concentrations from 20 to 250 $mg.L^{-1}$. The residual concentration of BF was measured using a UV–Vis spectrophotometer (PerkinElmer Optima) at a wavelength 543 nm. The adjustment of the pH of solution was achieved with 0.1 M HCl and 0.1 M NaOH and monitored by a pH meter (HANNA HI9812-5). The chemicals of analytical grade were purchased from Sigma–Aldrich-Fluka (Saint-Quentin, Fallavier, France).

2.2. Preparation of adsorbent

Chicken eggshell waste was obtained from local restaurant. Eggshells were washed several times with distilled water and then boiled in DDW for 10 min using Techno Water Bath in order to remove any residual impurities. Afterwards, ESM was carefully stripped from the eggshell manually. Subsequently, ESM was dried in Memmert Drying Oven at 50 °C for overnight and crushed into powder; only particles of size in the range 250–350 μm were used.

2.3. Characterization of adsorbent

The elemental analysis was performed with a CHNS-932 Leco instrument. Thermal analysis (TGA/DTA) was carried out by using Setaram setsys 1750 instrument in the temperature range 25–800 °C with a heating rate of 10 °C/min and under air atmosphere. The crystalline structure was characterized by X-ray diffraction (XRD) using Philips X'Pert diffractometer equipped with CuKα radiation source (λ = 1.5418 Å). Fourier Transform Infrared (FTIR) patterns were recorded to identify the functional groups of ESM using the IR Affinity-1S (SHIMADZU) in combination with a single reflection ATR under a maximum pressure of 0.1 GPa, standard resolution 4 cm^{-1} and an accumulation number of 50. The morphology of the ESM powder was analyzed by scanning electron microscopy (SEM) using JEM-2010-JEOL instrument. BET surface area was determined using a Nova Quantachrome Analyzer. The point of zero charge (pH_{PZC}) measurement was carried out by placing in various Erlenmeyer flasks 50 ml of 0.01 M NaCl solution and their pH (pH_i) was adjusted to different values between 2 and 12 by the addition of 0.1 M HCl or NaOH solutions. Then 100 mg of ESM powder was added into each solution and the mixture was filtered to remove the adsorbent and the filtrate was analyzed using a pH meter (pH_f) after 48 h.

2.4. Kinetic and equilibrium studies

Adsorption experiments in batch mode were performed in order to study the influence of the ESM dose, contact time, stirring speed, temperature, pH and dye initial concentration. During this study, 1.0 g of ESM was mixed in a set of 500 ml conical flasks each containing 200 ml of dye solution.

Batch tests were conducted at room temperature 25 ± 0.2 °C, pH solution (pH = 6) and concentration of 20 $mg.L^{-1}$. The flask was placed on a mechanical shaker and agitated at 150 rpm until equilibrium was attained. At the end of each adsorption experiment, the mixture of ESM and BF was centrifuged at 4000 rpm for 5 min. The absorbance of residual dye was analyzed using UV–Vis spectrophotometer. The adsorption experiments were repeated twice and the

Table 1
Elemental analysis for ESM.

Chemical composition (wt. %)	C	O	H	N	S
ESM	46.99	26.11	6.56	15.19	3.84

average standard deviation was found around 3%.

The quantity of dye adsorbed at equilibrium, Qe (mg.g^{-1}), was calculated using the following relationship:

$$Qe = \frac{(C_0 - C_e)\,V}{W} \quad (1)$$

where C_0 and C_e (mg.L^{-1}) are the initial and equilibrium concentration of dye, respectively; V (L) is the volume of dye solution and W (g) is the mass of ESM.

The dye removal rate (%) was calculated as follows:

$$R\,(\%) = \frac{(C_0 - C_t)}{C_0} \times 100 \quad (2)$$

where C_t (mg.L^{-1}) is the residual dye at time t (min).

3. Results and discussion

3.1. Characterizations

3.1.1. Chemical composition

Elemental analysis as shown in Table 1 reveals that ESM contains carbon, oxygen, hydrogen, nitrogen and sulfur; which indicates and confirms its protein nature with a high weight percentage of carbon (46.99%).

3.1.2. Thermo gravimetric and differential thermal analysis

A substance subjected to thermal treatment can undergo modifications of its physico-chemical properties as a phase change, a decomposition, a volume variation, a structural alteration, etc. (Hadfi et al., 2018). The TGA/DTA curves displayed in Fig. 1 (A) show that as the temperature rises, thermal decomposition of ESM powder at different degree occurred with the existence of the multistep decomposition. The first step of decomposition, corresponding to a weight loss of approximately 13.94% is observed around 61 °C and may be ascribed to the beginning of ESM denaturation of collagen (Choi et al., 2017).The second region in the range 155–540 °C results as a consequence of the thermal degradation of collagen (Torres et al., 2013). This effect can be associated with the ability of hydrogen belonging to water molecules to bond to amide groups (Torres et al., 2013). At 560 °C, all organics are removed corresponding to the total decomposition of ESM powder (Torres et al., 2013). In addition, it can be noticed the presence of endothermic and exothermic TDA peaks at 76.6 °C and 328.2 °C, respectively.

3.1.3. Structure analysis by XRD

The X-ray diffraction pattern of the ESM powder (Fig. 1 (B)) exhibits the presence of unique very broad peak at around 2θ = 20.36, indicating its amorphous nature, due to its chemical composition containing amides, amines and carboxylic compounds (Pant et al., 2017; Choi et al., 2017). This result is in agreement with the literature (Li et al., 2017b; Wang et al., 2016).

3.1.4. Structure analysis by FTIR

The FTIR spectrum of the ESM powder (Fig. 1 (C)) reveals several peaks that can be identified as follow: the peak at 3292 cm^{-1}corresponds to the OH and N–H stretching mode (amide A)

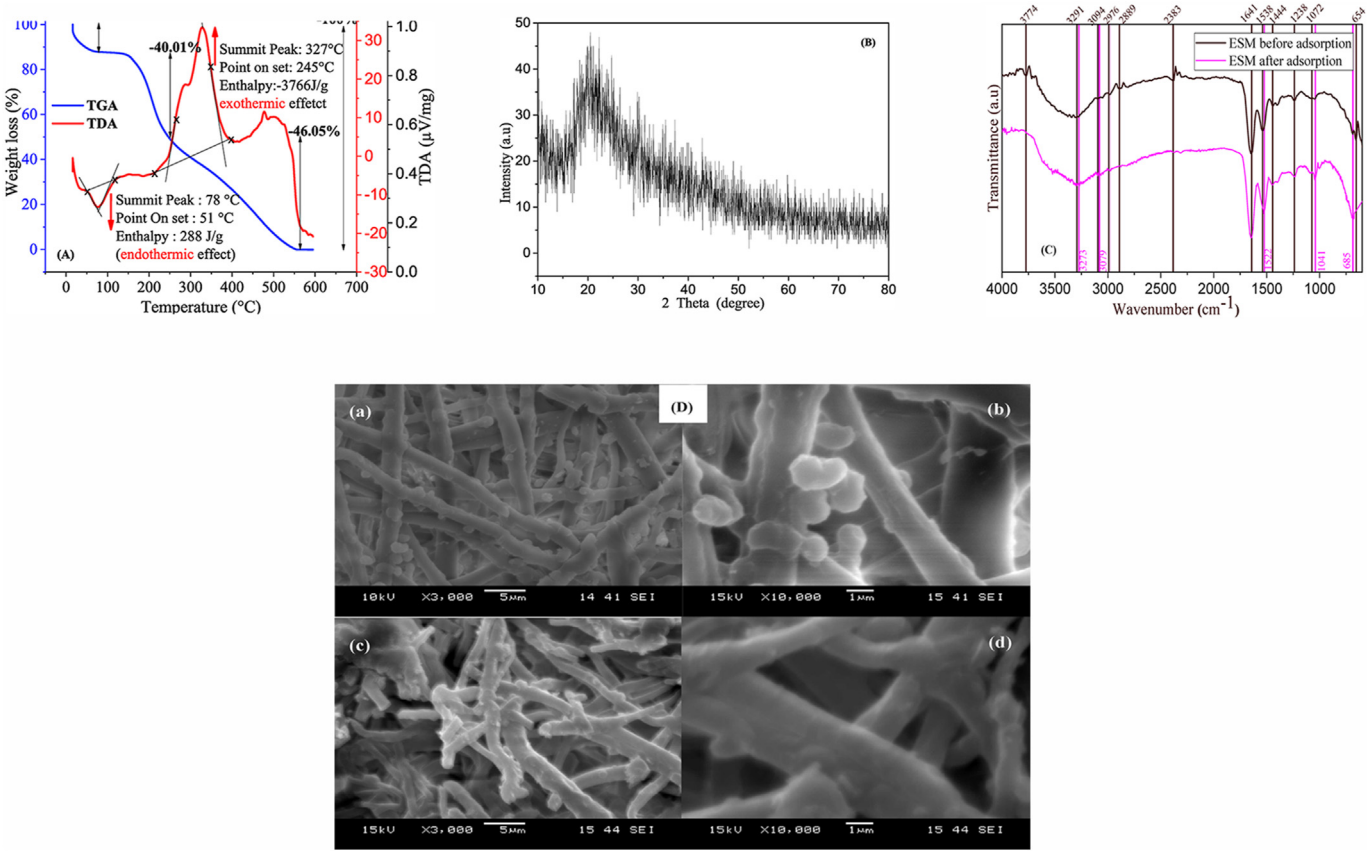

Fig. 1. Physico-chemical and structural characterization of ESM powder; (A) TGA/DTA curves; (B) X-ray diffraction pattern; (C) FTIR spectra (a) before and (b) after BF adsorption; (D) SEM images (a–b) before and (c–d) after BF adsorption.

Table 2
Chemical properties of ESM powder.

Characteristics	BET specific surface area ($m^2.g^{-1}$)	Pore volume ($cm^3.g^{-1}$) × 10^{-3}	Particle density ($g.cm^{-3}$)	Pore size (Å)
This study	11.56	6.173	1.001	12.27
Tsai et al. (2006)	1.053	7.1	2.658	-
Choi (2017)	4.45	69	-	34.5

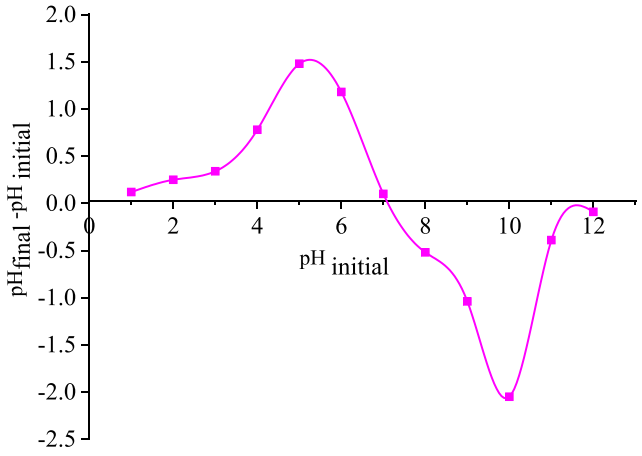

Fig. 2. Plot for the determination of point zero charge of the ESM powder.

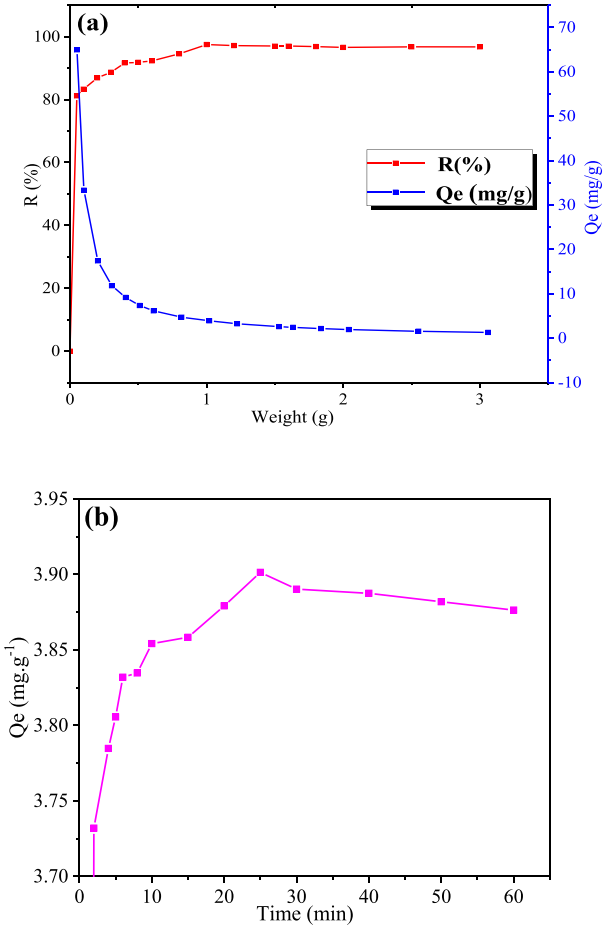

Fig. 3. Effect of adsorbent dose (a) and Effect of contact time (b) for the removal of BF onto ESM powder (V = 200 ml, pH = 6, C = 20 ppm, T = 25 °C).

(Liu et al., 2017); 3094, 2976 and 2889 cm^{-1} (C–H asymmetric stretching vibration in =C–H and $=CH_2$) associated with amide B (Sah and Pramanik, 2014; Li et al., 2017a, 2017b, 2017c); the peak of $–NH_2$ is appeared at 2383 cm^{-1} (Arief et al., 2008). The intense peak at 1642 cm^{-1} is associated with (C=O) (Baláž et al., 2016; Sah and Pramanik, 2014); the peak at 1539 cm^{-1} associated with CN stretching/NH bending modes; the peak at 1239 cm^{-1} corresponding to CN stretching/NH bending modes are assigned to the amide I, amide II and amide III vibrations of the glycoprotein, respectively (Baláž et al., 2016; Sah and Pramanik, 2014); the bands at 1444, 1072, 664 cm^{-1} are due to (C=C), (C–O) and (C–S) stretching mode, respectively (Li et al., 2017c).

On the other hand, after BF adsorption, the following changes occurred: (i) a decrease in the intensity and a slight shift in the position of some peaks for instance –OH and N–H: 3273 cm^{-1}, C=O: 1522 cm^{-1}, amine C–N: 1065 cm^{-1}; (ii) the disappearance of three peaks,$–NH_2$ and C–H were located at 2383 cm^{-1} and 2889 cm^{-1}, respectively.

The observed changes signify that an interaction occurred between the BF dye functional groups and ESM particles surface such as the exchange reaction between the dye molecules and H^+ of functional groups, an indication that a chemisorption process occurred.

3.1.5. SEM observations

SEM images of ESM powder before adsorption (Fig. 1 D (a-b)) illustrates a network-type microstructure formed by intercrossed fibers arranged randomly (Wu et al., 2001; Ehrampoush et al., 2011). The diameter of fibers varies in a broad range within the microscale, while the size of particles ranges in a narrow range around 1 μm. This fibrous proteins-network indicates that the organic matrix of the eggshell membrane is not rigid compared to inorganic minerals.

However, after the BF adsorption (Fig. 1 D (c-d)), there is a swelling of ESM protein fibers meanwhile there is porosity loss of ESM surface resulting from the accumulation of BF molecules.

The results of BET specific surface area of ESM powder are reported in Table 2. It is found that the surface area is about 11.56 $m^2.g^{-1}$ and the pore diameter of 12.27 Å, which indicates that the material is microporous according to IUPAC (An et al., 2013). The size of BF molecule is around 11.34 Å, which is smaller than the pore size of 12.27 Å; hence it could penetrate easily within the microstructure of the substrate. Moreover, it is important to highlight that the specific area value of ESM powder in this study is greater than the values reported in the literature by Tsai et al. (2006) and Choi (2017), which signifies a much higher adsorption capacity is expected.

3.1.6. Determination of pH_{PZC}

The point of zero charge (PZC) represents the solution pH in which the surface is neutrally charged (Schreier et al., 2010), and its position defines the affinity of the surface to the ionic species (Kosmulski, 2014). The difference between the initial and final pH (pH_f-pH_i) has been plotted against the initial pH (pH_i) and the point where pH_f - pH_i = 0 is taken as the pH_{pzc} (Fig. 2). The value of pH_{pzc} of ESM powder is found to be 7.05. This implies that at pH < pH_{PZC} = 7.05, the ESM surface has a positive charge and negative charge at pH > pH_{PZC} = 7.05. Hence, at pH values below the PZC, –OH, –COOH and $–NH_2$ groups protonates and become positively charged, while above the PZC they deprotonates and become negatively charged, thus increasing the attraction of dye ions with positive charge and favoring significantly the

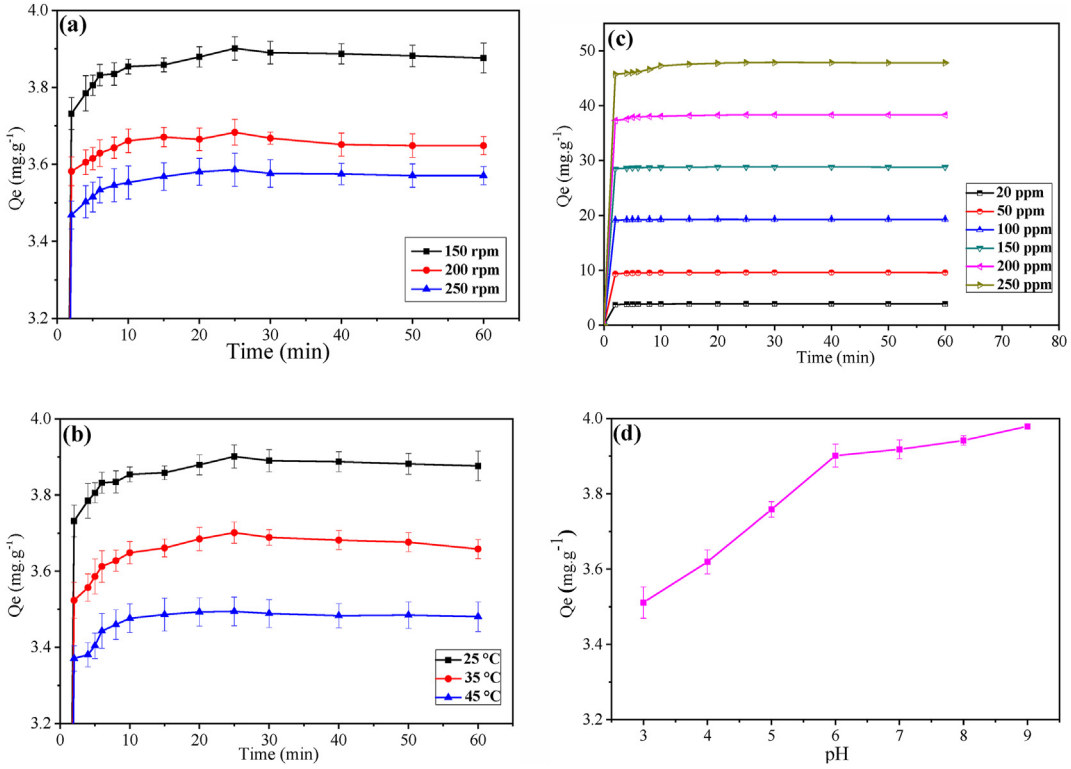

Fig. 4. Effects of speed (a); temperature (b); initial concentration (c) and pH (d) on the adsorption of the BF dye on ESM.

Table 3
Values of the kinetic constants for the adsorption of the BF dye on ESM.

	q_{exp}(mg.g^{-1})	Pseudo-first order			Pseudo-second order		
		q_e	k_1	R^2	q_e	k_2	R^2
Effect of Initial BF Concentration (ppm)							
20	3.901	6.196	0.100	0.922	3.891	3.476	1
50	9.612	1.352	0.182	0.983	9.615	0.315	1
100	19.058	2.603	0.152	0.975	19.600	0.128	1
150	28.816	1.561	0.180	0.989	29.410	0.435	1
200	38.333	0.676	0.133	0.959	38.460	1.109	1
250	47.858	0.133	0.190	0.972	50.000	4.353	1
Effect of Temperature (°C)							
25	3.901	6.196	0.100	0.922	3.891	3.476	1
35	3.701	5.245	0.214	0.974	3.690	5.245	1
45	3.494	5.454	0.268	0.980	3.496	0.277	1
Effect of pH							
3	3.511	3.923	0.097	0.949	3.484	0.209	0.999
4	3.619	6.394	0.145	0.986	4.610	0.143	1
5	3.758	2.809	0.159	0.981	3.773	0.182	1
6	3.901	6.196	0.100	0.922	3.891	3.476	1
7	3.918	2.501	0.128	0.980	3.921	0.179	1
8	3.941	5.865	0.125	0.983	3.937	0.104	1
9	3.979	10.50	0.098	0.804	3.984	0.059	1

adsorption process.

3.2. Batch adsorption measurements

3.2.1. Effect of adsorbent dose

The variation of dye removal percentage with respect to the adsorbent dose, as clearly illustrated in Fig. 3 (a), can be divided into three stages: (i) a drastic reduction in the adsorption capacity up to 0.25 mg corresponding to a significant increase in the removal percentage; (ii) gradual decrease up to 1.0 g to end up attaining (iii) a stationary stage for higher doses. This can be attributed to the presence of a large number of free functional groups during the early stage of reaction alongside with numerous active sites thereby facilitating the interaction with dye molecules and consequently adsorption occurs (Nandi et al., 2009b). Nonetheless, too more active sites may exceed the demand when the adsorption process reaches saturation, hence certain active sites are effectively unused resulting in a relative decline of the adsorption capacity (Arias et al., 1991). Similar observations were reported in the literature for the adsorption of BF onto anionic polyacrylamide/graphene oxide aerogels (Zhang et al., 2017). Therefore, the following experiments have been carried out at a fixed adsorbent dose of 1 g.

3.2.2. Effect of contact time

The equilibrium time plays a key role in the design of economic wastewater treatment systems (Gupta and Saleh, 2013).To evaluate the effect of the reaction time on the adsorption of BF dye on ESM, the experiments are preceded by varying shaking time from 2 to 60 min. From Fig. 3 (b), it can be observed that the rate of BF dye removal is high during the initial stage of contact time (2 min) followed by a slow rise until reaching equilibrium. The achieved high adsorption capacity can be associated with the rise in the adsorption driving force as a result of the intense concentration gradient occurring relatively to the increase in the initial concentration. Therefore, a reaction time of 25 min has been chosen as the optimum value for future experiments.

3.2.3. Effect of stirring speed

The rotation speed is also considered as an important parameter in the adsorption process, especially for dye adsorption, since it has a direct influence on the distribution of the solute in the bulk solution (Nandi et al., 2009a). Three stirring speed values have been studied, i.e. 150, 200 and 250 rpm. According to Fig. 4 (a), it is clear that the adsorption efficiency of BF slightly decreases for higher stirring speed, with the observation of the superposition of speed curves at 200 and 250 rpm, which indicates that the retention capacity of the membrane is not influenced in the high stirring speeds. Therefore, the optimum stirring speed of 150 rpm is fixed for the future experiments.

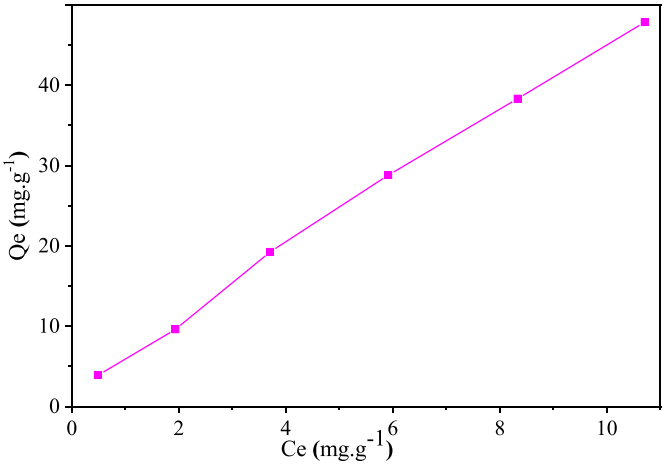

Fig. 5. Equilibrium isotherm of BF adsorption onto ESM.

3.2.4. Effect of temperature

The influence of medium temperature on the adsorption rate of BF onto ESM has been explored at 25, 35 and 45 °C, and the results are presented in Fig. 4 (b) and Table 3. It can be noticed that the adsorbed amount of BF decreases moderately from 3.901 to 3.494 mg.g^{-1}when the temperature rises from 25 to 45 °C. This can be associated with the acceleration in the molecular motion when the temperature in increased, as a result the electrostatic effect becomes less effective. In addition to that, the intermolecular hydrogen bond existing between BF and ESM will break, thereby reducing the adsorption efficiency (Li et al., 2013a; Yuan et al., 2017).The as-obtained results demonstrate that the adsorption process is dominantly exothermic. Therefore, 25 °C has been chosen to be the optimum temperature for further studies.

3.2.5. Effect of BF concentration

The effect of initial BF concentration on the adsorption process has been evaluated in the range 20–250 ppm at pH 6 and temperature of 25 °C. The obtained results are illustrated in Fig. 4 (c) and Table 3. It can be seen there is a sharp rise in the amount of the adsorbed BF from 3.901 to 47.858 mg g^{-1} as the BF concentration increases from 20 to 250 ppm. Herein, it is important to mention that the increase in the initial concentration of the dye provides an effective driving force to overcome all resistance of pollutant migration from the aqueous solution to the ESM surface (Ehrampoush et al., 2011; Elkady et al., 2011; Kumar et al., 2010). In addition, the high adsorption efficiency can be justified by the porous nature and the specific surface area of ESM; in addition, functional groups such as amine and carboxyl groups present in ESM can react with BF molecules which results in better fixation onto its surface. On the other hand, it is worth noting that the increase in BF initial concentration does not affect the percent BF removal for ESM; the efficiency remains within the range 96.1–97.8%.

3.2.6. Effect of pH

In the literature, it has been reported that the value of the pH often plays an important role during the adsorption process (An and Huang, 2012); both the surface charge of adsorbent and the degree of ionization of dye molecules are affected by the variation of solution pH (Zhang et al., 2017). The effect of initial pH on BF adsorption has been carried out by varying the pH from 3 to 9 for an initial BF concentration of 20 mg.L^{-1} and at 25 °C. From Table 3 and Fig. 4 (d), it can be noticed that in the pH interval 3–9, the amount of adsorbed BF increases gradually and appreciably with increasing pH to reach the highest BF absorption capacity of 3.997 mg g^{-1} for a pH of 9. This can be explained as follow: the surface charges of ESM change from negative to positive when value of pH_{ZPC} becomes higher and lower respectively. In this case, the large numbers of H^+ present at low pH will protonate the amino groups onto the surface of ESM (Sun et al., 2012).

Meanwhile, due to its basic nature, BF will generate cationic pigment (BF^+) in the aqueous solution, which inhibits the adsorption of cationic dye in the solution particularly for much lower pH value (Srinivasan et al., 2006). Moreover, for higher pH value, the presence of more OH^- ions will favor deprotonating much easier –NH_2, resulting in the enhancement of the adsorption rate, thanks to the electrostatic attraction between these two oppositely charged ions.

Similar results were also found in the adsorption of cationic dye by ESM (Salman et al., 2012).

3.3. Kinetics effect of adsorption

The adsorption kinetics has been identified as an important factor for scheming the adsorption process and plays a key role for optimizing the experimental factors influencing adsorbent-adsorbate interactions (Öztürk and Malkoc, 2014). The aim of this study is to determine the order of the adsorption kinetics; hence two models shave been considered for testing the obtained experimental data and thus elucidate the kinetics of the adsorption process.

- ***Pseudo first-order-model***

The linearized form of the Lagergren, (1898) pseudo first-order-model is more compatible with low solute concentrations. The linear form of this model is represented by the following equation:

$$Ln(q_e - q_t) = Lnq_e - K_1 t \quad (3)$$

with K_1 is the rate constant for first order adsorption kinetics (min^{-1}), q_t and q_e are the adsorption capacities at time t and at equilibrium (mg.g^{-1}), respectively.

- ***Pseudo second-order-model***

This model (Ho and McKay, 1998) has been adopted to explain the sorption kinetics. It is assumed that the adsorption follows second order chemisorption, and can be described by the linearized former presented by the following relation:

$$\frac{t}{q_t} = \frac{1}{K_2 q_e^2} + \frac{1}{q_e} t \quad (4)$$

where K_2 is the pseudo-second-order adsorption rate constant (g.mg^{-1}.min^{-1}).

The kinetics parameters obtained by fitting the kinetic data of BF adsorption onto ESM are given in Table 3. Based on the linear

Table 4
Plots for Langmiur (a), Freundlich (b) and Temkin (c) isotherms for BF adsorption on ESM.

Model									
Langmuir				Freundlich			Temkin		
Q_{exp}^{max} (mg.g^{-1})	q_m (mg.g^{-1})	b (mg.g^{-1})	R^2	n	K_F (mg.g^{-1})	R^2	A_T (L.g^{-1})	B_T (J.mol^{-1})	R^2
47.858	111.111	0.159	0.982	1.206	6.475	0.992	1.700	13.780	0.861

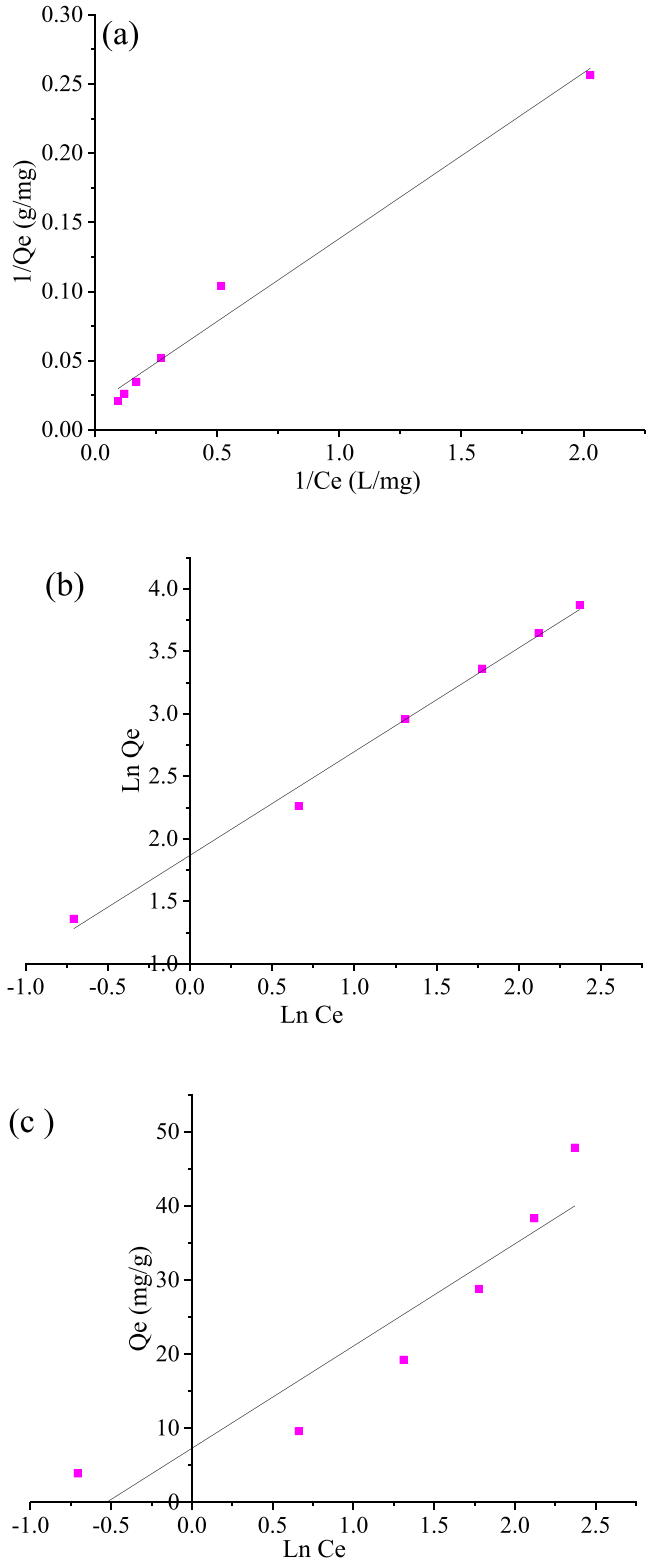

Fig. 6. Plots for Langmiur (a), Freundlich (b) and Temkin (c) isotherms for BF adsorption.

regression correlation coefficient R^2 values, the best-fit model will be selected. From this table, the correlation coefficients (R^2) are found to be highest for pseudo-second order compared to that of the pseudo-first order; i.e. R^2 values are equal or very close to the unity (1 or 0.999). In addition, the experimental and calculated values of Q_e are found almost similar. Accordingly, the kinetics of BF dye adsorption onto ESM follows a pseudo-second order model, implying that the chemisorption is rate-determining step for controlling the adsorption process (Chen et al., 2011; Bhattacharyya and Gupta, 2011) and emphasis that chemisorption was the dominant mechanism and involved valence forces through the exchange or sharing of electrons between the binding sites on the ESM and dye molecules (Sun et al., 2016).In this study, chemical bonds can be formed by the electrostatic attraction of functional groups in ESM (such as –OH, –SH, –COOH and $–NH_2$) (Pant et al., 2017). Similar results have been observed by Sun et al. (2016) and Maity et al. (2018).

3.4. Adsorption isotherm

Adsorption isotherms can provide in-depth information on adsorbate/adsorbent interactions, which is identified by certain constant values that provides insight son surface characteristics and affinity of the adsorbent. In this case, there exists relationship between the quantities of adsorbed dye and that remaining in aqueous solution at equilibrium for a constant temperature. As shown in Fig. 5, the shape of the curves Qe vs. Ce clearly indicates that the obtained isotherm belongs to C-type, according to the classification of equilibrium isotherm in solution as postulated by Giles et al., (1960). This means that the C curve is characterized by the constant partitioning of solute between solution and substrate, and the linearity indicates that the number of adsorption sites remains constant: the more solute is adsorbed more sites will be created (Giles et al., 1960).

In this study, the experimental data are analyzed according to the Langmuir, Freundlich and Temkin isotherm models in order to demonstrate the relation of BF dye adsorbed amount and its equilibrium concentration (Cui et al., 2015). The correlation coefficients (R^2) are used to determine the best-fitted isotherm models.

- ***Langmuir isotherm***

This model assumes that adsorption occurs by monolayer and that all adsorption sites at the adsorbent are homogeneous. It is expressed by a linear equation (Song et al., 2017):

$$\frac{1}{Q_e} = \frac{1}{Q_m} + \frac{1}{k_L \times Q_m} * \frac{1}{C_e} \quad (6)$$

where $\boldsymbol{Q_m}$ ($mg.g^{-1}$) defines the maximum adsorption efficiency and $\boldsymbol{k_L}$ ($L.mg^{-1}$) represents the dependency-constant. The maximum adsorption efficiency and Langmuir constant will be computed from the slope and intercept of the linear plots $\frac{1}{Qe}$ vs. $\boldsymbol{C_e}$, thereby providing a direct line of slope $\frac{1}{Q_m}$ that is compatible to full monolayer coverage ($mg.g^{-1}$) while the intercept represents the quantity $\frac{1}{k_L \times Q_m}$.

- ***Freundlich isotherm***

This model has been developed according to an empirical equation to describe various systems. It presumes that the multilayer of the adsorption process occurs on a heterogeneous surface and its linear form can be presented as follow (Fu et al., 2015):

$$\ln Q_e = \ln k_F + \frac{1}{n} \ln C_e \quad (7)$$

where $\boldsymbol{k_F}$ ($mg.g^{-1}$) is the Freundlich constant being indicative of adsorption capacity, and n is the Freundlich constant (index of adsorption intensity or surface heterogeneity). The values of $\boldsymbol{k_F}$ and **n** are obtained from the linear plot $\ln Q_e$ *vs.* $\ln C_e$.

- ***Temkin isotherm***

This model is based on two main assumptions, namely (i) the

Table 5
Comparison of adsorption capacities of BF onto various adsorbents.

Adsorbent	Adsorption capacity ($mg.g^{-1}$)	Reference
Euryale ferox salisbury seed shell	19.48	Kalita et al. (2017)
Super absorbent polymer	11.7	Dhodapkar et al. (2007)
Bottomash	9.15	Gupta et al. (2008)
Monodispersed mesoporous silica nanoparticles	14.70	Qin et al. (2017)
Iron-manganese oxide coated kaolinite	10.36	Khan and Khan (2015)
Guar gum bonded	24	Zhang et al. (2012)
Calcined mussel shell (CMS)	141.65	El Haddad (2016)
Starch -capped zinc selenide nanoparticles loaded on activated carbon (ST -Zn -Se -NPs –AC)	222.7	Sharifpour et al. (2020)
Graphite oxide	1.834	Qin et al. (2014)
Raw pistachio nutshells (RPNS)	118.2	El-Azazy et al. (2019)
Deoiled soya	13	Gupta et al. (2008)
Polymeric nanocomposite	0.439	Kaith et al. (2019)
ESM	47.858	This study

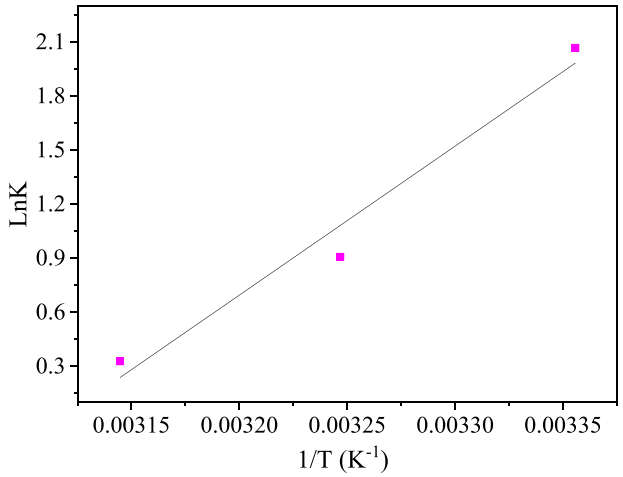

Fig. 7. Linear plot of lnKvs.1/T for the sorption of BF on ESM at 298, 308 and 318 K.

Table 6
Thermodynamic parameters for the adsorption of BF onto ESM at different temperatures.

T (K)	ΔG° ($kJ.mol^{-1}$)	ΔH° ($kJ.mol^{-1}$)	ΔS° ($kJ.mol^{-1}.K^{-1}$)
298	−5.124	−68.948	−0.214
308	−2.324		
318	−0.856		

adsorbent/adsorbate interaction cannot be neglected during the adsorption mechanism; (ii) the heat of adsorption decreases linearly with the adsorbate coverage and caused by the interaction. Its linear equation can be expressed as follow (Wong et al., 2019):

$$Q_e = B_T lnA_T + B_T lnC_e \quad (8)$$

where $B = \frac{RT}{b_T}$, b_T ($J.mol^{-1}$) is the heat of adsorption, A_T ($L.g^{-1}$) is the Temkin isotherm equilibrium binding constant, R is the gas constant (8.314 $J\ mol^{-1}.K^{-1}$), T is the absolute temperature. The values of B_T and A_T will be determined from the slope and intercept of the plot *Qe vs.* ln Ce, respectively.

The adsorption capacity of ESM powder as illustrated in Fig. 4 (c), increases gradually when the dye concentration in the aqueous phase increases, which can be due to the heterogeneous surface of ESM. On the other hand, the SEM image of ESM after adsorption (Fig. 1 D (c-d)) shows the formation of net multi-layers of adsorbed dye molecules with a non-uniform adsorption distribution meanwhile the concentration of the dye molecules on the surface is completely heterogeneous. The results obtained through the three mathematical model equations are presented in Table 4 and Fig. 6. The correlation of models becomes less significant. It can be observed that the Freundlich adsorption isotherm model is the most suitable (R^2 = 0.992), whereas Langmuir and Temkin models deviate from the obtained data having (R^2 = 0.982) and (R^2 = 0.861), respectively.

It is important to compare the obtained results with literature (Kalita et al., 2017; Dhodapkar et al., 2007; Gupta et al., 2008; Qin et al., 2017; Khan and Khan, 2015; Zhang et al., 2012; Kaith et al., 2019). Table 5 shows a brief summary of adsorption capacities of some adsorbents for BF removal compared with ESM powder used in this study. It is noteworthy that the ESM powder exhibits a much higher adsorption capacity for BF removal compared to others adsorbents reported in the literature. This can be associated with its network-fibrous and microporous microstructure with relatively high surface area.

Meanwhile, other materials in the literature showed high adsorption rate (El Haddad, 2016; Sharifpour et al., 2020; El-Azazy et al., 2019), as shown in Table 5. However, the reported materials are fabricated from expensive components (such as Na_2SeSO_3, $Zn(O_2CCH_3)_2$) and require complex/lengthy synthesis routes including separation by sedimentation, drying for long time (up to 72 h), calcination (1173 K for 2 h then 673 K for 4 h), chemical reactions (longer time and complex chemical reactions during synthesis which usually affect the purity of final products) for nanoparticles synthesis and so on.

Also, it is important to consider other factors such as the contact time and kinetics: (i) the maximum rate is achieved after 120 min for RPNS, 100 min for CMS, and 6 min for ST-Zn-Se-NPs-AC compared to only 25 min for ESM in this study; (ii) the kinetics parameter proves that all these adsorbents obey pseudo-second-order, the adsorption rate constant K_2 is found to be $9.03*10^{-3}$ g $mg^{-1}.min^{-1}$ for RPNS, $35.67*10^{-4}$ g $mg^{-1}.min^{-1}$ for CMS, and 1.77 g $mg^{-1}.min^{-1}$ for ST-Zn-Se-NPs-AC, thereby indicating clearly much slower adsorption kinetics compared to ESM with 4.353 g $mg^{-1}.min^{-1}$.

3.5. Thermodynamic study

The investigation of the influence of temperature during adsorption measurements will help in identifying the type and spontaneity of adsorption processes related to BF dye. In this study, the temperature has been varied in the range 298–318 K. According to the obtained results, it is found that the extent of BF adsorption is significantly affected by the solution temperature.

The thermodynamic parameters, namely the changes in free energy (ΔG°), enthalpy (ΔH°), and entropy (ΔS°) associated with the adsorption process, can be determined by using the following equations (Wong et al., 2019; Kumari et al., 2016):

$$\Delta G^\circ = -R.\ T.LnKc \quad (11)$$

$$\Delta G^\circ = \Delta H^\circ - T.\ \Delta S^\circ \quad (12)$$

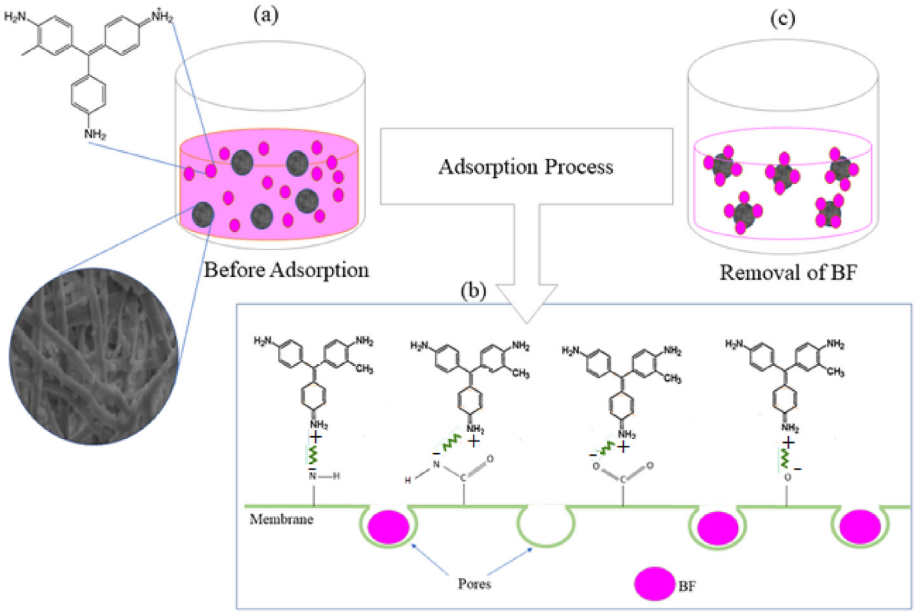

Fig. 8. Proposed mechanism for the adsorption of BF by ESM powder.

The values of ΔH° and ΔS° correspond to the slope and intercept respectively of the linear plot Ln Kc vs. of $\frac{1}{T}$. Fig. 7 displays the linear plot lnKc vs. 1/T and the corresponding thermodynamic parameters are given in Table 6. The change in Gibbs free energy (ΔG°) shows a negative value, indicating the feasibility of the adsorption process and its spontaneous nature for the adsorption of BF onto ESM powder. The values of ΔG° are −5.124, −2.324, and −0.856 kJ.mol^{-1} for 298, 308 and 318 K respectively. These values also confirmed the adsorption to be a physical process with the physisorption in the range (−20)– (0.0) kJ.mol^{-1}, while a value in the range (−80) – (−400) kJ.mol^{-1} corresponds to chemisorption process (Li et al., 2013b).The negative value of ΔH^0 signifies the exothermic nature of the reaction occurring during the adsorption process. Meanwhile, the negative value of the entropy (ΔS^0) indicates a reduction in randomness between the solid-solution interfaces during the adsorption process, suggesting as well that the system exhibits random behavior. Similar results of adsorption of dyes onto different adsorbents with a negative change in entropy and enthalpy have been reported (Liu et al., 2014).

3.6. Adsorption mechanism

For adsorptions studies, the foremost challenge is to propose possible mechanism to better understand all possible involved reactions/interactions during adsorption process. In this context, several experimental factors have been identified to play key role in the adsorption mechanism thereby have to be considered, namely but not limited to, the nature and complexity of the adsorbate structure, the existence of functional groups, the microstructure (particle size, shape of particle, porosity, agglomeration level) and surface chemistry (charge, available sites) of the adsorbent, in addition to the adsorbent/adsorbate specific interactions.

According to BET analysis, it has been found that the size of the BF molecule is smaller than the pore size; it can therefore penetrate within the microstructure of the substrate. The presence of such pores is responsible for the adsorption of higher amount of BF. The combination of the experimental findings of the present study (kinetic adsorption data well adapted by the pseudo-second order model), FTIR analysis in addition to the structure and microstructure of both adsorbate and adsorbent, the proposed mechanism for BF adsorption by ESM possibly involves: (i) chemical forces and chemical bonds formed by the electrostatic interactions between the negatively charged ESM and positively charged dye molecules. That is, the glycoproteins of ESM are made up of large amounts of amino, carboxyl and hydroxyl groups, which act as directing and capping functions of ESM for cationic dye; (ii) the hydrophilic anionic groups present on ESM surface are responsible for extraction and transport of cationic dye ions.

In addition, according to the obtained results, the adsorption rate is found to enhance for higher pH resulting in an electrostatic attraction between the chromophore groups of dye and the negatively charged ESM surface. Moreover, ESM possesses an isoelectric point at pH 7.05 with a positive/negative zeta potential values corresponding to pH lower/higher than 7.05. In the acidic medium, the functional groups of ESM such as amino, carboxylic, hydroxyl and so on are protonated, and as result its surface becomes positively charged (Zulfikar and Setiyanto 2013; Manera et al., 2018), as can be expressed by the following reactions:

$$ESM - NH_2 + H^+ \leftrightarrow ESM - NH_3^+$$

$$ESM - CO - NH_2 + H^+ \leftrightarrow ESM - CO - NH_3^+$$

$$ESM - OH + H^+ \leftrightarrow ESM - OH_2^+$$

$$ESM - COOH + H^+ \leftrightarrow ESM - COOH_2^+$$

The presence of positive charges onto ESM adsorbent surface will inhibit the adsorption of the cationic dye. In addition, in basic medium the number of active sites on ESM increases, and the following reactions occur spontaneously:

$$ESM - OH + OH^- \leftrightarrow ESM - O^- + H_2O$$

$$ESM - COOH + OH^- \leftrightarrow ESM - COO^- + H_2O$$

$$ESM - NH_2 + OH^- \leftrightarrow ESM - NH^- + H_2O(\text{amino deprotonate})$$

$$ESM - CO - NH_2 + OH^- \leftrightarrow ESM - CO - NH^- + H_2O(\text{amido deprotonate})$$

At higher pH value, the surface of ESM becomes negatively charged, and consequently the electrostatic forces of the positively charged BF cations will enhance the attraction and this situation can be summarized by the following reactions:

$$ESM - O^- + BF^+ \leftrightarrow ESM - O- BF$$

$$ESM - COO^- + BF^+ \leftrightarrow ESM - COO - BF$$

$ESM - NH^{-} + BF^{+} \leftrightarrow ESM - NH - BF$

$ESM - CO - NH^{-} + BF^{+} \leftrightarrow ESM - CO - NH - BF$

This is plausible mechanism of cationic dye adsorption by ESM. A schematic representation of the proposed mechanism is displayed in Fig. 8.

4. Conclusion

The present work aimed at valorizing eggshell waste by exploring its membrane for the removal a toxic dye (BF). The results of this study demonstrated that powdered eggshell waste can be employed as an alternative adsorbent for BF removal from water. ESM exhibited high porosity and surface area, therefore, showed a relatively high adsorption performance. The amount of adsorbed BF was found to increase significantly with its initial concentration. The effect of stirring speed and pH had a slight positive influence on the retention capacity of BF onto ESM. Surprisingly, the rise of temperature decreased the adsorption efficiency. The kinetic adsorption data were well adapted by the pseudo-second order model, indicating that the adsorption process occurs by chemisorption. The adsorption of BF molecules using ESM biosorbent obeyed Freundlich adsorption isotherm. The thermodynamic parameters revealed that the adsorption was spontaneous and exothermic. This detailed study demonstrated that low cost and eco-friendly potential bioadsorbent prepared from agricultural waste exhibited outstanding capability for the removal of BF dye from their aqueous solutions and hence, can be a viable alternative to commercial use and could present a future potential for the removal of other organic contaminants.

CRediT authorship contribution statement

Wahiba Bessashia: Validation, Investigation, Resources, Writing - original draft, Writing - review & editing, Visualization. **Yamina Berredjem:** Conceptualization, Methodology, Resources, Supervision. **Zhour Hattab:** Conceptualization, Methodology, Resources, Supervision. **Mohamed Bououdina:** Validation, Writing - original draft, Writing - review & editing, Visualization, Supervision.

Declaration of competing interest

The authors declare that they have no known competing financial interests or personal relationships that could have appeared to influence the work reported in this paper.

References

Abdel-Khalek, M.A., Abdel Rahman, M.K., Francis, A.A., 2017. Exploring the adsorption behavior of cationic and anionic dyes on industrial waste shells of egg. J. Environ. Chem. Eng. 5 (1), 319–327. https://doi.org/10.1016/j.jece.2016.11.043.

An, Chunjiang, Huang, Guohe, 2012. Stepwise adsorption of phenanthrene at the fly ash–water interface as affected by solution chemistry: experimental and modeling studies. Environ. Sci. Technol. 46 (22), 12742–12750. https://doi.org/10.1021/es3035158.

An, Feng-Hua, Cheng, Yuan-Ping, Wu, Dong-Mei, Wang, Liang, 2013. The effect of small micropores on methane adsorption of coals from Northern China. Adsorption 19 (1), 83–90. https://doi.org/10.1007/s10450-012-9421-3.

Arias, Jose L., Fernandez, Maria S., Dennis, James E., Caplan, Arnold I., 1991. Collagens of the chicken eggshell membranes. Connect. Tissue Res. 26 (1–2), 37–45. https://doi.org/10.3109/03008209109152162.

Arief, Vicentius Ochie, Trilestari, Kiki, Jaka Sunarso, Indraswati, Nani, Ismadji, Suryadi, 2008. Recent progress on biosorption of heavy metals from liquids using low cost biosorbents: characterization, biosorption parameters and mechanism studies. Clean - Soil, Air, Water 36 (12), 937–962. https://doi.org/10.1002/clen.200800167.

Asfaram, Arash, Ghaedi, Mehrorang, Hajati, Shaaker, Goudarzi, Alireza, Alipanahpour Dil, Ebrahim, 2017. Screening and optimization of highly effective ultrasound-assisted simultaneous adsorption of cationic dyes onto Mn-doped Fe3O4-nanoparticle-loaded activated carbon. Ultrason. Sonochem. 34, 1–12. https://doi.org/10.1016/j.ultsonch.2016.05.011.

Baláž, Matej, 2014. Eggshell membrane biomaterial as a platform for applications in materials science. Acta Biomater. https://doi.org/10.1016/j.actbio.2014.03.020.

Baláž, Matej, Jana, Ficeriová, Briančin, Jaroslav, 2016. Influence of milling on the adsorption ability of eggshell waste. Chemosphere 146, 458–471. https://doi.org/10.1016/j.chemosphere.2015.12.002.

Bayramoglu, Gulay, Altintas, Begum, Yakup Arica, M., 2009. Adsorption kinetics and thermodynamic parameters of cationic dyes from aqueous solutions by using a new strong cation-exchange resin. Chem. Eng. J. 152 (2–3), 339–346. https://doi.org/10.1016/j.cej.2009.04.051.

Bhattacharyya, Krishna G., Gupta, Susmita Sen, 2011. Removal of Cu (II) by natural and acid-activated clays: an insight of adsorption isotherm, kinetic and thermodynamics. Desalination 272 (1–3), 66–75. https://doi.org/10.1016/j.desal.2011.01.001.

Cao, L., Kang, Z.W., Ding, Q., Zhang, X., Lin, H., Lin, M., Yang, D.P., 2020. Rapid pyrolysis of Cu^{2+}-polluted eggshell membrane into a functional Cu^{2+}-Cu^{+} / biochar for ultrasensitive electrochemical detection of nitrite in water. Sci. Total Environ. 723, 138008. https://doi.org/10.1016/j.scitotenv.2020.138008.

Chen, Rongzhi, Zhi, Chunyi, Yang, Huang, Bando, Yoshio, Zhang, Zhenya, Sugiur, Norio, Golberg, Dmitri, 2011. Arsenic (V) adsorption on Fe3O4 nanoparticle-coated boron nitride nanotubes. J. Colloid Interface Sci. 359 (1), 261–268. https://doi.org/10.1016/j.jcis.2011.02.071.

Choi, Hee Jeong, 2017. Use of methyl esterified eggshell membrane for treatment of aqueous solutions contaminated with anionic sulfur dye. Water Sci. Technol. 76 (10), 2638–2646. https://doi.org/10.2166/wst.2017.346.

Choi, Jawun, Pant, Bishweshwar, Lee, Chohye, Park, Mira, Park, Soo Jin, Kim, Hak Yong, 2017. Preparation and characterization of eggshell membrane/PVA hydrogel via electron beam irradiation technique. J. Ind. Eng. Chem. 47, 41–45. https://doi.org/10.1016/j.jiec.2016.11.014.

Choi, Yoonah, Zheng, Ting, 2019. Fluorophores with tailored multiple functionalities for biomedical, agricultural and environmental. Mol. Syst. Des. Eng. https://doi.org/10.1039/c9me00086k.

Chung, Sheng Heng, Manthiram, Arumugam, 2014. Carbonized eggshell membrane as a natural polysulfide reservoir for highly reversible Li-S batteries. Adv. Mater. 26 (9), 1360–1365. https://doi.org/10.1002/adma.201304365.

Cui, Limei, Guo, Xiaoyao, Qin, Wei, Wang, Yaoguang, Gao, Liang, Yan, Liangguo, Yan, Tao, Du, Bin, 2015. Removal of mercury and methylene blue from aqueous solution by xanthate functionalized magnetic graphene oxide: sorption kinetic and uptake mechanism. J. Colloid Interface Sci. 439, 112–120.

D'Souza, S.F., Jitendra, Kumar, Sandeep, Kumar Jha, Kubal, B.S., 2013. Immobilization of the urease on eggshell membrane and its application in biosensor. Mater. Sci. Eng. C 33 (2), 850–854. https://doi.org/10.1016/j.msec.2012.11.010.

da Silva, Romário Justino, Lima, Ravi M.A.P., de Oliveira, Mário César Albuquerque, Alcaraz-Espinoza, José J., de Melo, Celso Pinto, de Oliveira, Helinando P., 2019. Supercapacitors based on (carbon nanostructure)/PEDOT/(Eggshell membrane) electrodes. J. Electroanal. Chem. 856, 113658. https://doi.org/10.1016/j.jelechem.2019.113658.

Dhodapkar, Rita, Rao, N.N., Pande, S.P., Nandy, T., Devotta, Sukumar, 2007. Adsorption of cationic dyes on Jalshakti®, super absorbent polymer and photocatalytic regeneration of the adsorbent. React. Funct. Polym. 67 (6), 540–548. https://doi.org/10.1016/j.reactfunctpolym.2007.03.0.

Ding, Qi, Kang, Zewen, Cao, Liping, Lin, Mengshi, Lin, Hetong, Yang, Da Peng, 2020. Conversion of waste eggshell into difunctional Au/CaCO3 nanocomposite for 4-nitrophenol electrochemical detection and catalytic reduction. Appl. Surf. Sci. 510, 145526. https://doi.org/10.1016/j.apsusc.2020.145526.

Ehrampoush, M., Ghanizadeh, G.H., Ghaneian, M., 2011. Equilibrium and kinetics study of reactive red 123 dye removal from aqueous solution by adsorption on eggshell. J. Environ. Heal. Sci. Eng. 8 (2), 101–106.

El-Azazy, Marwa, El-Shafie, Ahmed S., Ashraf, Aya, Issa, Ahmed A., 2019. Eco-structured biosorptive removal of basic fuchsin using pistachio nutshells: a definitive screening design-based approach. Appl. Sci. (Switzerland) 9 (22). https://doi.org/10.3390/app9224855.

El Haddad, Mohammadine, 2016. Removal of basic fuchsin dye from water using mussel shell biomass waste as an adsorbent: equilibrium, kinetics, and thermodynamics. J. Taibah Univ. Sci. 10 (5), 664–674. https://doi.org/10.1016/j.jtusci.2015.08.007.

El-Khateeb, M.A., Al-Herrawy, A.Z., Kamel, M.M., El-Gohary, F.A., 2009. Use of wetlands as post-treatment of anaerobically treated effluent. Desalination 245 (1–3), 50–59. https://doi.org/10.1016/j.desal.2008.01.071.

Elkady, M.F., M Ibrahim, Amal, Abd El-Latif, M.M., 2011. Assessment of the adsorption kinetics, equilibrium and thermodynamic for the potential removal of reactive red dye using eggshell biocomposite beads. Desalination 278 (1–3), 412–423. https://doi.org/10.1016/j.desal.2011.05.063.

Fu, Jianwei, Chen, Zhonghui, Wang, Minghuan, Liu, Shujun, Zhang, Jinghui, Zhang, Jianan, Han, Runping, Xu, Qun, 2015. Adsorption of methylene blue by a high-efficiency adsorbent (polydopamine microspheres): kinetics, isotherm, thermodynamics and mechanism analysis. Chem. Eng. J. 259, 53–61. https://doi.org/10.1016/j.cej.2014.07.101.

Giles, C.H., MacEwan, T.H., Nakhwa, S.N., Smith, D., 1960. 786. Studies in adsorption. Part XI. A system of classification of solution adsorption isotherms, and its use in diagnosis of adsorption mechanisms and in measurement of specific surface areas of solids. J. Chem. Soc. (Resumed). https://doi.org/10.1039/jr9600003973. 3973–93.

Gupta, V.K., Mittal, Alok, Gajbe, Vibha, Mittal, Jyoti, 2008. Adsorption of basic fuchsin using waste materials—bottom ash and deoiled soya—as adsorbents. J. Colloid Interface Sci. 319 (1), 30–39. https://doi.org/10.1016/j.jcis.2007.09.091.

Gupta, Vinod K., Saleh, Tawfik A., 2013. Sorption of pollutants by porous carbon, carbon nanotubes and fullerene-an overview. Environ. Sci. Pollut. Control Ser. 20 (5), 2828–2843. https://doi.org/10.1007/s11356-013-1524-1.

Hadfi, Abdallah, Ben Aazza, Said, Belattar, M'barek, Mohareb, Said, Ali, Driouiche, 2018. Study of the physico-chemical quality of the water of irrigation in biougra circle along with highlighting the effectiveness of an inhibitor of calcium carbonate

precipitation. Mediterr. J. Chem. https://doi.org/10.13171/mjc74181121-hadfi.
Han, Runping, Wang, Yu, Zhao, Xin, Wang, Yuanfeng, Xie, Fuling, Cheng, Junmei, Tang, Mingsheng, 2009. Adsorption of methylene blue by phoenix tree leaf powder in a fixed-bed column: experiments and prediction of breakthrough curves. Desalination 245 (1–3), 284–297. https://doi.org/10.1016/j.desal.2008.07.013.
He, Xingsheng, Yang, Da-peng, Zhang, Xiaoyan, Liu, Minghuan, Kang, Zewen, Lin, Chenfei, 2019. Waste eggshell membrane-templated CuO-ZnO nanocomposites with enhanced adsorption , catalysis and antibacterial properties for water puri Fi cation. Chem. Eng. J. 369 (March), 621–633. https://doi.org/10.1016/j.cej.2019.03.047.
Ho, Y.S., McKay, G., 1998. The kinetics of sorption of basic dyes from aqueous solution by sphagnum moss peat. Can. J. Chem. Eng. 76 (4), 822–827. https://doi.org/10.1002/cjce.5450760419.
Kaith, Singh, Balbir, Shanker, Uma, Gupta, Bhuvanesh, 2019. One-pot green synthesis of polymeric nanocomposite: biodegradation studies and application in sorption-degradation of organic pollutants. J. Environ. Manag. 234https://doi.org/10.1016/j.jenvman.2018.12.117. 345–56.
Kalita, S., Pathak, M., Devi, G., Sarma, H.P., Bhattacharyya, K.G., Sarma, A., Devi, A., 2017. Utilization of euryale ferox salisbury seed shell for removal of basic fuchsin dye from water: equilibrium and kinetics investigation. RSC Adv. 7 (44), 27248–27259. https://doi.org/10.1039/c7ra03014b.
Khan, Tabrez A., Khan, Equbal A., 2015. Removal of basic dyes from aqueous solution by adsorption onto binary iron-manganese oxide coated kaolinite: non-linear isotherm and kinetics modeling. Appl. Clay Sci. 107, 70–77. https://doi.org/10.1016/j.clay.2015.01.005.
Khelaifia, Fatma Zohra, Hazourli, Sabir, Nouacer, Sana, Rahima, Hachani, Ziati, Mounir, 2016. Valorization of raw biomaterial waste-date stones-for Cr (VI) adsorption in aqueous solution: thermodynamics, kinetics and regeneration studies. Int. Biodeterior. Biodegrad. 114, 76–86. https://doi.org/10.1016/j.ibiod.2016.06.002.
Kong, Jiaojiao, Huang, Lihui, Yue, Qinyan, Gao, Baoyu, 2014. Preparation of activated carbon derived from leather waste by H3PO4 activation and its application for basic fuchsin adsorption. Desalin. Water Treat. 52 (13–15), 2440–2449. https://doi.org/10.1080/19443994.2013.794713.
Kosmulski, Marek, 2014. The PH dependent surface charging and points of zero charge. VI. Update. J. Colloid Interface Sci. 426 (1), 209–212. https://doi.org/10.1016/s0021-9797(04)00170-5.
Kumar, P Senthil, C Vincent, K Kirthika, Sathish Kumar, K., 2010. Kinetics and equilibrium studies of Pb2+ in removal from aqueous solutions by use of nano-silversol-coated activated carbon. Braz. J. Chem. Eng. 27 (2), 339–346. https://doi.org/10.1590/s0104-66322010000200012.
Kumari, H Jayasantha, Krishnamoorthy, P., Arumugam, T.K., Radhakrishnan, S., Vasudevan, D., 2016. An efficient removal of crystal violet dye from waste water by adsorption onto TLAC/chitosan composite: a novel low cost adsorbent. Int. J. Biol. Macromol. https://doi.org/10.1016/j.ijbiomac.2016.11.077.
Kyzas, George Z., Lazaridis, Nikolaos K., Ch Mitropoulos, Athanassios, 2012. Removal of dyes from aqueous solutions with untreated coffee residues as potential low-cost adsorbents: equilibrium, reuse and thermodynamic approach. Chem. Eng. J. https://doi.org/10.1016/j.cej.2012.02.045.
Lagergren, Svenska, 1898. About the theory of so-called adsorption of soluble substances. K. - Sven. Vetenskapsakademiens Handl. 24 (4), 1–39.
Li, Huiqin, Huang, Guohe, An, Chunjiang, Hu, Jingtao, Yang, Siqi, 2013a. Removal of tannin from aqueous solution by adsorption onto treated coal fly ash: kinetic, equilibrium, and thermodynamic studies. Ind. Eng. Chem. Res. 52 (45), 15923–15931. https://doi.org/10.1021/ie402054w.
Li, Yanhui, Du, Qiuju, Liu, Tonghao, Sun, Jiankun, Wang, Yonghao, Wu, Shaoling, Wang, Zonghua, Xia, Yanzhi, Xia, Linhua, 2013b. Methylene blue adsorption on graphene oxide/calcium alginate composites. Carbohydr. Polym. 95 (1), 501–507. https://doi.org/10.1016/j.carbpol.2013.01.094.
Li, Yaling, Ye, Yong, Fan, Yunde, Zhou, Ji, Jia, Li, Tang, Bin, Wang, Xungai, 2017a. Silver nanoprism-loaded eggshell Membrane : a facile platform for in situ SERS monitoring of catalytic reactions. Crystals 7 (2), 45. https://doi.org/10.3390/cryst7020045.
Li, Yaling, Zhou, Ji, Fan, Yunde, Ye, Yong, Tang, Bin, 2017b. Preparation of environment-friendly 3D eggshell membrane-supported anatase TiO2 as a reusable photocatalyst for degradation of organic dyes. Chem. Phys. Lett. 689, 142–147. https://doi.org/10.1016/j.cplett.2017.10.019.
Li, Ying, Wang, Anyi, Bai, Yunfei, Wang, Shiping, 2017c. Evaluation of a mixed anionic–nonionic surfactant modified eggshell membrane as an advantageous adsorbent for the solid-phase extraction of Sudan I–IV as model analytes. J. Separ. Sci. 40 (12), 2591–2602. https://doi.org/10.1002/jssc.201700094.
Li, Chen, Zhang, Meihan, Song, Chengwen, Tao, Ping, Sun, Menghan, Shao, Mihua, Wang, Tonghua, 2018a. Enhanced treatment ability of membrane technology by integrating an electric field for dye wastewater treatment: a review. J. AOAC Int. 101 (5), 1341–1352. https://doi.org/10.5740/jaoacint.18-0050.
Li, Xiaoyun, Ma, Meihu, Ahn, Dong Uk, Huang, Xi, 2018b. Preparation and characterization of novel eggshell membrane-chitosan blend films for potential wound-care dressing: from waste to medicinal products. Int. J. Biol. Macromol. 123, 477–484. https://doi.org/10.1016/j.ijbiomac.2018.10.215.
Li, Xiaoyun, Cai, Zhaoxia, Ahn, Dong Uk, Huang, Xi, 2019. Development of an antibacterial nanobiomaterial for wound-care based on the absorption of AgNPs on the eggshell membrane. Colloids Surf. B Biointerfaces 183, 110449. https://doi.org/10.1016/j.colsurfb.2019.110449.
Li, Zhanhai, Yang, Da Peng, Chen, Yisong, Du, Zhongyi, Guo, Yunlong, Huang, Jiale, Li, Qingbiao, 2019. Waste eggshells to valuable Co3O4/CaCO3 materials as efficient catalysts for VOCs oxidation. Mol. Catal. 483https://doi.org/10.1016/j.mcat.2020.110766. November 2020.
Liu, Menglong, Luo, Gaoxing, Wang, Yuzhen, Xu, Rui, Wang, Ying, He, Weifeng, Tan, Jianglin, Xing, Malcolm, Wu, Jun, 2017. Nano-silver-decorated microfibrous eggshell membrane: processing, cytotoxicity assessment and optimization, antibacterial activity and wound healing. Sci. Rep. 7 (1), 436. https://doi.org/10.1038/s41598-017-00594-x.
Liu, N., Liu, T., 2011. Adsorption and decoloration of nitroso dye based on eggshell membrane. Adv. Mater. Res. 183–185, 963–966. https://doi.org/10.4028/www.scientific.net/AMR.183-185.963.
Liu, Qingquan, Chen, Xiaoyu, Kang, Ze-Wen, Zheng, Chaohui, Yang, Da-Peng, 2020. Facile synthesis of eggshell membrane-templated Au/CeO 2 3D nanocomposite networks for nonenzymatic electrochemical dopamine sensor. Nanoscale Res. Lett. 15 (1), 1–10. https://doi.org/10.1186/s11671-019-3203-8.
Liu, Xueyan, An, Shuai, Zhou, Xinyu, Zhang, Lei, Zhang, Yunyu, Wen, Shi, Yang, Jichun, 2014. Comparative studies of removal of methyl green and basic fuchsin from wastewater by a novel magnetic nanoparticles Mg-ferrites. J. Dispersion Sci. Technol. 35 (12), 1727–1736. https://doi.org/10.1080/01932691.2013.871553.
Maity, Jyoti Prakash, Chun Mei, Hsu, Lin, Tz Jiun, Wen Chien, Lee, Bhattacharya, Prosun, Bundschuh, Jochen, Chen, Chien Yen, 2017. Removal of fluoride from water through bacterial-surfactin mediated novel hydroxyapatite nanoparticle and its efficiency assessment: adsorption isotherm, adsorption kinetic and adsorption thermodynamics. Environ. Nanotechnol. Monit. Manag. 9, 18–28. https://doi.org/10.1016/j.enmm.2017.11.001. November 2018.
Manera, Christian, Piroli Tonello, Andrezza, Perondi, Daniele, Godinho, Marcelo, 2018. Adsorption of leather dyes on activated carbon from leather shaving wastes: kinetics, equilibrium and thermodynamics studies. Environ. Technol. 1–13. https://doi.org/10.1080/09593330.2018.1452984.
Nandi, B.K., Goswami, A., Purkait, M.K., 2009a. Removal of cationic dyes from aqueous solutions by kaolin: kinetic and equilibrium studies. Appl. Clay Sci. 42 (3–4), 583–590. https://doi.org/10.1016/j.clay.2008.03.015.
Nandi, Barun Kumar, Goswami, Amit, Kumar Purkait, Mihir, 2009b. Adsorption characteristics of brilliant green dye on kaolin. J. Hazard Mater. 161 (1), 387–395. https://doi.org/10.1016/j.jhazmat.2008.03.110.
Nouacer, S., S Hazourli, R Djellabi, Z Khelaifia, F., Hachani, R., Ziati, M., 2016. Using a new lignocellulosic material based on palm stems for hexavalent chromium adsorption in aqueous solution. Int. J. Environ. Res. 10 (1), 41–50.
Öztürk, A., Malkoc, E., 2014. Adsorptive potential of cationic basic yellow 2 (BY2) dye onto natural untreated clay (NUC) from aqueous phase: mass transfer analysis, kinetic and equilibrium profile. Appl. Surf. Sci. 299, 105–115. https://doi.org/10.1016/j.apsusc.2014.01.193.
Pant, Bishweshwar, Park, Mira, Kim, Hak Yong, Park, Soo Jin, 2017. CdS-TiO2NPs decorated carbonized eggshell membrane for effective removal of organic pollutants: a novel strategy to use a waste material for environmental remediation. J. Alloys Compd. https://doi.org/10.1016/j.jallcom.2016.12.360.
Postai, Debora Luiza, Demarchi, Carla Albertina, Zanatta, Francielle, Caroline Cipriani Melo, Danielle, Antonio Rodrigues, Clóvis, 2016. Adsorption of rhodamine B and methylene blue dyes using waste of seeds of Aleurites moluccana, a low cost adsorbent. Alexandria Eng. J. 55 (2), 1713–1723. https://doi.org/10.1016/j.aej.2016.03.017.
Pramanpol, Nuttawan, Nitayapat, Nuttakan, 2006. Adsorption of reactive dye by eggshell and its membrane. Kasetsart J. - Natural Sci. 40 (Suppl. L), 192–197.
Preda, N., Costas, A., Enculescu, M., Enculescu, I., 2020. Biomorphic 3D fibrous networks based on ZnO , CuO and ZnO – CuO composite nanostructures prepared from eggshell membranes. Mater. Chem. Phys. 240, 122205. https://doi.org/10.1016/j.matchemphys.2019.122205.
Qin, Jiao, Qiu, Fengxian, Rong, Xinshan, Yan, Jie, Zhao, Hao, Yang, Dongya, 2014. Removal of basic fuchsin dye from aqueous solutions using graphite oxide modified aromatic polyurethane foam material. Toxicol. Environ. Chem. 96 (6), 849–860. https://doi.org/10.1080/02772248.2014.993642.
Qin, Peige, Yang, Yixin, Zhang, Xiaoting, Niu, Jiahua, Yang, Hui, Tian, Shufang, 2017. Highly efficient , rapid , and simultaneous removal of cationic dyes from aqueous solution using monodispersed mesoporous silica nanoparticles as the adsorbent. https://doi.org/10.3390/nano8010004.
Quadrado, Rafael F.N., Fajardo, André R., 2017. Fast decolorization of azo methyl orange via heterogeneous fenton and fenton-like reactions using alginate-Fe2 + /Fe3 + films as catalysts. Carbohydr. Polym. 177, 443–450. https://doi.org/10.1016/j.carbpol.2017.08.083.
Rahman, Nafisur, Khan, Mohammad Fazeel, 2016. Nitrate removal using poly-o-toluidine zirconium(IV) ethylenediamine as adsorbent: batch and fixed-bed column adsorption modelling. J. Water Process Eng. 9, 254–266. https://doi.org/10.1016/j.jwpe.2016.01.007.
Sadaf, Sana, Bhatti, Haq Nawaz, Nausheen, Sana, Noreen, Saima, 2014. Potential use of low-cost lignocellulosic waste for the removal of direct violet 51 from aqueous solution: equilibrium and breakthrough studies. Arch. Environ. Contam. Toxicol. https://doi.org/10.1007/s00244-013-9992-3.
Sah, Mahesh Kumar, Pramanik, Krishna, 2014. Soluble-eggshell-membrane-protein-modified porous silk fibroin scaffolds with enhanced cell adhesion and proliferation properties. J. Appl. Polym. Sci. 131 (8). https://doi.org/10.1002/app.40138. n/a–n/a.
Saleh, Rosari, Taufik, Ardiansyah, 2019. Degradation of methylene blue and Congo-red dyes using fenton, photo-fenton, sono-fenton, and sonophoto-fenton methods in the presence of iron (II, III) oxide/zinc oxide/graphene (Fe3O4/ZnO/graphene) composites. Separ. Purif. Technol. 210, 563–573. https://doi.org/10.1016/j.seppur.2018.08.030.
Salman, Dhuha D., Ulaiwi, Wisam S., Tariq, N.M., 2012. Determination the optimal conditions of methylene blue adsorption by the chicken egg shell membrane. Int. J. Poultry Sci. 11 (6), 391–396. https://doi.org/10.3923/ijps.2012.391.396.
Schreier, Marc, E Feltes, Theresa, Schaal, Melanie T., Regalbuto, John R., 2010. The determination of oxide surface charging parameters for a predictive metal adsorption

model. J. Colloid Interface Sci. 348 (2), 571–578. https://doi.org/10.1016/j.jcis.2010.04.064.
Sharifpour, Ebrahim, Ghaedi, Mehrorang, Asfaram, Arash, Farsadrooh, Majid, Alipanahpour Dil, Ebrahim, Javadian, Hamedreza, 2020. Modeling and optimization of ultrasound-assisted high performance adsorption of basic fuchsin by starch-capped zinc selenide nanoparticles/AC as a novel composite using response surface methodology. Int. J. Biol. Macromol. 152, 913–921. https://doi.org/10.1016/j.ijbiomac.2020.02.236.
Shen, Kai, Gondal, M.A., 2017. Removal of hazardous rhodamine dye from water by adsorption onto exhausted coffee ground. J. Saudi Chem. Soc. 21, S120–S127. https://doi.org/10.1016/j.jscs.2013.11.005.
Song, Kaili, Xu, Helan, Xu, Lan, Xie, Kongliang, Yang, Yiqi, 2017. Cellulose nanocrystal-reinforced keratin bioadsorbent for effective removal of dyes from aqueous solution. Bioresour. Technol. 232, 254–262. https://doi.org/10.1016/j.biortech.2017.01.070.
Srinivasan, Madhavi, Ferraris, Cristiano, White, Tim, 2006. Cadmium and lead ion capture with three dimensionally ordered macroporous hydroxyapatite. Environ. Sci. Technol. 40 (22), 7054–7059. https://doi.org/10.1021/es060972s.
Sun, Ling, Yu, Hongwen, Fugetsu, Bunshi, 2012. Graphene oxide adsorption enhanced by in situ reduction with sodium hydrosulfite to remove acridine orange from aqueous solution. J. Hazard Mater. 203–204, 101–110.
Sun, Zhiming, Yao, Guangyuan, Liu, Mingyi, Zheng, Shuilin, 2016. Adsorbent and its efficient removal of cationic dyes. J. Taiwan Inst. Chem. Eng. 71, 501–509. https://doi.org/10.1016/j.jtice.2016.12.013.
Torres, Fernando G., Troncoso, Omar P., Franco, Piaggio, Hijar, Alfredo, 2010. Structure-property relationships of a biopolymer network: the eggshell membrane. Acta Biomater. 6 (9), 3687–3693. https://doi.org/10.1016/j.actbio.2010.03.014.
Torres, Fernando G., Troncoso, Omar P., Montes, Maribella R., 2013. The effect of temperature on the mechanical properties of a protein-based biopolymer network. J. Therm. Anal. Calorim. 111 (3), 1921–1925. https://doi.org/10.1007/s10973-012-2915-0.
Tsai, W.T., Yang, J.M., Lai, C.W., Cheng, Y.H., Lin, C.C., Yeh, C.W., 2006. Characterization and adsorption properties of eggshells and eggshell membrane. Bioresour. Technol. 97 (3), 488–493. https://doi.org/10.1016/j.biortech.2005.02.050.
Uliana, Carolina V., Garbellini, Gustavo S., Yamanaka, Hideko, 2012. Electrochemical reduction of disperse orange 1 textile dye at a boron-doped diamond electrode. J. Appl. Electrochem. 42 (5), 297–304. https://doi.org/10.1007/s10800-012-0403-7.
Ummartyotin, S., Pisitsak, P., Pechyen, C., 2016. Eggshell and bacterial cellulose composite membrane as absorbent material in active packaging. Int. J. Polym. Sci. https://doi.org/10.1155/2016/1047606.
Verma, Akshaya Kumar, Dash, Rajesh Roshan, Bhunia, Puspendu, 2012. A review on chemical coagulation/flocculation technologies for removal of colour from textile wastewaters. J. Environ. Manag. 93 (1), 154–168. https://doi.org/10.1016/j.jenvman.2011.09.012.
Wang, Na, Ma, Zhennan, Zhou, Shutao, Guo, Liang, 2016. Facile fabrication of SERS substrate based on food residue eggshell membrane. Chem. Phys. Lett. 666, 45–50. https://doi.org/10.1016/j.cplett.2016.10.077.
Wang, Shaomang, Li, Dinglong, Sun, Cheng, Yang, Shaogui, Guan, Yuan, He, Huan, 2014. Synthesis and characterization of G-C3N4/Ag3VO4 composites with significantly enhanced visible-light photocatalytic activity for triphenylmethane dye degradation. Appl. Catal. B Environ. 144, 885–892. https://doi.org/10.1016/j.apcatb.2013.08.008.
Wang, Weidong, Chen, Bo, Huang, Yuming, Cao, Jia, 2010. Evaluation of eggshell membrane-based bio-adsorbent for solid-phase extraction of linear alkylbenzene sulfonates coupled with high-performance liquid chromatography. J. Chromatogr. A 1217 (36), 5659–5664. https://doi.org/10.1016/j.chroma.2010.07.017.
Wong, Syieluing, Hasnaa, H Tumari, Ngadi, Norzita, Balqis Mohamed, Nurul, Hassan, Onn, Mat, Ramli, Nor Aishah Saidina, Amin, 2019. Adsorption of anionic dyes on spent tea leaves modified with polyethyleneimine (PEI-STL). J. Clean. Prod. 206, 394–406. https://doi.org/10.1016/j.jclepro.2018.09.201.
Wu, Feng-Chin, Tseng, Ru-Ling, Juang, Ruey-Shin, 2001. Kinetic modeling of liquid-phase Adsorption of reactive dyes and metal ions on chitosan. Water Res. 35 (3), 613–618. https://doi.org/10.1016/s0043-1354(00)00307-9.
Yuan, Junjie, Qiu, Fengxian, Li, Pingping, 2017. Synthesis and characterization of β -cyclodextrin – carboxymethyl cellulose – graphene oxide composite materials and its application for removal of basic fuchsin. J. Iran. Chem. Soc. 14 (9), 1827–1837. https://doi.org/10.1007/s13738-017-1122-0.
Zeyada, H.M., Makhlouf, M.M., Ismail, M.I.M., Salama, A.A., 2015. Thermal behavior , structure formation and optical characteristics of nanostructured basic fuchsine thin Fi lms. Mater. Chem. Phys. 163, 45–53. https://doi.org/10.1016/j.matchemphys.2015.07.013.
Zhang, Xiuju, Zheng, Shaojie, Lin, Zhidan, Tan, Shaozao, 2012. Preparation of guar gum bonded with B-cyclodextrin microspheres and the absorption on basic fuchsine. J. Appl. Polym. Sci. 123 (4), 2250–2256. https://doi.org/10.1002/app.33875.
Zhang, Yan, Huang, Guohe, Chunjiang, An, Xiaying, Xin, Xia, Liu, Maya, Raman, Yao, Yao, Wenxia, Wang, Mukesh, Doble, 2017. Transport of anionic azo dyes from aqueous solution to gemini surfactant-modified wheat bran: synchrotron infrared, molecular interaction and adsorption studies. Sci. Total Environ. 595, 723–732. https://doi.org/10.1016/j.scitotenv.2017.04.031.
Zhang, Xiaoyan, He, Xingsheng, Kang, Zewen, Cui, Malin, Yang, Da-Peng, Luque, Rafael, 2019. Waste eggshell-derived dual-functional CuO/ZnO/eggshell nanocomposites: (photo) catalytic reduction and bacterial inactivation. ACS Sustain. Chem. Eng. 7 (18), 15762–15771. https://doi.org/10.1021/acssuschemeng.9b04083.
Zhang, Xiaohui, Liu, Minghuan, Kang, Zewen, Wang, Bingqing, Wang, Bo, Jiang, Fuyi, Wang, Xiansong, Yang, Da Peng, Luque, Rafael, 2020a. NIR-triggered photocatalytic/photothermal/photodynamic water remediation using eggshell-derived CaCO3/CuS nanocomposites. Chem. Eng. J. 388, 124304. https://doi.org/10.1016/j.cej.2020.124304.
Zhang, Xiaoyan, Huang, Jialun, Kang, Zewen, Yang, Da Peng, Luque, Rafael, 2020b. Eggshell-Templated synthesis of PbS/CaCO3 nanocomposites for [Rad]CO3− mediated efficient degradation of tetracycline under solar light irradiation. Mol. Catal. 484 (November 2019), 110786. https://doi.org/10.1016/j.mcat.2020.110786.
Zulfikar, Muhammad Ali, Setiyanto, Henry, 2013. Adsorption of Congo red from aqueous solution CTAB-kaolin from bechar Algeria. Int. J. ChemTech Res. 5 (October), 1532–1540. https://doi.org/10.4236/jsemat.2014.46037.